J|A|C|S
ARTICLES
Published on Web 07/11/2002

Significant Enhancement of Electron Transfer Reduction of NAD^+ Analogues by Complexation with Scandium Ion and the Detection of the Radical Intermediate−Scandium Ion Complex

Shunichi Fukuzumi,* Osamu Inada, Naoya Satoh, Tomoyoshi Suenobu, and Hiroshi Imahori†

Contribution from the Department of Material and Life Science, Graduate School of Engineering, Osaka University, CREST, Japan Science and Technology Corporation (JST), Suita, Osaka 565-0871, Japan

Received February 26, 2002

Abstract: 4-Acetyl-*N,N*-diisopropyl-1-benzylnicotinamidinium ion ($ABNA^+$) and 1-benzyl-4-phenylnicotinamidinium ion ($PhBNA^+$) were newly synthesized as NAD^+ analogues to examine the electron-transfer reactivity and the effects of metal ions on the reactivity in comparison with those of 1-benzylnicotinamidinium ion (BNA^+) and 1-methyl-4-phenylpyridinium ion (MPP^+) which has no amide or acetyl group. A remarkable positive shift in the one-electron reduction potential of $ABNA^+$ was observed in the presence of Sc^{3+} which forms a 1:1 complex with $ABNA^+$ through both acetyl and amide groups, whereas no such shift in the presence of Sc^{3+} was observed for the one-electron reduction of MPP^+ which has no acetyl or amide group. Similar but less positive shifts in the one-electron reduction potentials were observed in the presence of Sc^{3+} for the one-electron reduction of BNA^+ and $PhBNA^+$ both of which have only one amide group. The rate of electron-transfer reduction of $ABNA^+$ is enhanced significantly by the complexation with Sc^{3+} to produce stable $ABNA^{\bullet}$-Sc^{3+} complex which has been successfully detected by ESR. The electron self-exchange rates of the $MPP^{\bullet}/MPP^+$ system have been determined from the ESR line width variation and are compared with those of the $ABNA^{\bullet}/ABNA^+$ system.

Introduction

A variety of biological redox reactions are mediated by nicotinamide adenine dinucleotide (NAD^+) and the reduced form (NADH).[1] The effects of metal ions on oxidation of NADH analogues have attracted considerable interest in relation to the essential role of metal ions in the redox reactions of nicotinamide coenzymes in the native enzymatic system.[2−5] The essential roles of metal ions have also been well recognized in a variety of enzymatic functions.[6−9] In contrast to well-known coordination of metal ions to NADH analogues,[3,4,10] few attempts have been made heretofore to examine the effects of metal ions on reduction of NAD^+ or NAD^+ analogues.[11] Thus, there has so far been no report on the complex formation between metal ions and NAD^+ analogues or the one-electron reduced radical species. Due to the instability of the radicals, no ESR spectrum of $NAD^{\bullet}$ radical analogues has ever been reported.[12,13] As such, the spin distributions of $NAD^{\bullet}$ radical analogues or the effects of metal ions on the electron-transfer reduction of NAD^+ analogues have yet to be clarified.

* To whom correspondence should be addressed. E-mail: fukuzumi@ap.chem.eng.osaka-u.ac.jp.

† Present address: Department of Molecular Engineering, Graduate School of Engineering, Kyoto University, PRESTO, Japan Science and Technology Corporation, Sakyo-ku, Kyoto 606-8501, Japan.

(1) Voet, D.; Voet, J. G. *Biochemistry, 2nd ed.*; John Wiley & Sons: New York, 1995.
(2) (a) Eisner, U.; Kuthan, J. *Chem. Rev.* **1972**, *72*, 1. (b) Stout, D. M.; Meyers, A. I. *Chem. Rev.* **1982**, *82*, 223.
(3) (a) Sigman, D. S.; Hajdu, J.; Creighton, D. J. In *Bioorganic Chemistry*; van Tamelen, E. E., Ed.; Academic Press: New York, 1978; Vol. IV, p 385. (b) Gase, R. A.; Pandit, U. K. *J. Am. Chem. Soc.* **1979**, *101*, 7059. (c) Ohno, A.; Yamamoto, H.; Oka, S. *J. Am. Chem. Soc.* **1981**, *103*, 2041.
(4) (a) Fukuzumi, S. In *Advances in Electron-Transfer Chemistry*; Mariano, P. S., Ed.; JAI press; Greenwich, CT, 1992; pp 67−175. (b) Fukuzumi, S.; Tanaka, T. In *Photoinduced Electron Transfer*; Fox, M. A., Chanon, M., Eds.; Elsevier: Amsterdam, 1988; Part C, Chapter 10.
(5) (a) Fukuzumi, S.; Koumitsu, S.; Hironaka, K.; Tanaka, T. *J. Am. Chem. Soc.* **1987**, *109*, 305. (b) Fukuzumi, S.; Tokuda, Y.; Kitano, T.; Okamoto, T.; Otera, J. *J. Am. Chem. Soc.* **1993**, *115*, 8960. (c) Fukuzumi, S.; Ohkubo, K.; Tokuda, Y.; Suenobu, T. *J. Am. Chem. Soc.* **2000**, *122*, 4286.
(6) (a) Lippard, S. J.; Berg, J. M. *Principles of Bioinorganic Chemistry*; University Science Books: Mill Valley, California, 1994. (b) Hughes, M. N. *The Inorganic Chemistry of Biological Processes, 2nd ed.*; John Wiley & Sons: New York, 1984.
(7) (a) Itoh, S.; Kumei, H.; Nagatomo, S.; Kitagawa, T.; Fukuzumi, S. *J. Am. Chem. Soc.* **2001**, *123*, 2165. (b) Lassmann, G.; Eriksson, L. A.; Lendzian, F.; Lubitz, W. *J. Phys. Chem. A* **2000**, *104*, 9144.
(8) (a) Clarke, M. J. *Comments Inorg. Chem.* **1984**, *3*, 133. (b) Kaim, W.; Schwederski, B. *Bioinorganic Chesmitry: Inorganic Elements in the Chemistry of Life*; John Wiley & Sons: Chichester, 1994.
(9) Fukuzumi, S.; Tanaka, T. In *Photoinduced Electron Transfer*; Fox, M. A., Chanon, M., Eds.; Elsevier: Amsterdam, 1988; Part C, Chapter 11.
(10) Fukuzumi, S.; Itoh, S. *Antioxid. Redox Signaling* **2001**, *3*, 807.
(11) For the reduction of NAD^+ analogues by metal complexes, see: (a) Konno, H.; Sakamoto, K.; Ishitani, O. *Angew. Chem., Int. Ed.* **2000**, *39*, 4061. (b) Kobayashi, A.; Takatori, R.; Kikuchi, I.; Konno, H.; Sakamoto, K.; Ishitani, O. *Organometallics* **2001**, *16*, 3361. (c) Lo, H. C.; Buriez, O.; Kerr, J. B.; Fish, R. H. *Angew. Chem., Int. Ed.* **1999**, *38*, 1429. (d) Lo, H. C.; Leiva, C.; Buriez, O.; Kerr, J. B.; Olmstead, M. M.; Fish, R. H. *Inorg. Chem.* **2001**, *40*, 6705
(12) (a) Hapiot, P.; Moiroux, J.; Savéant, J. M. *J. Am. Chem. Soc.* **1990**, *112*, 1337. (b) Forster, R. J. *Phys. Chem. Chem. Phys.* **1999**, *1*, 1543.
(13) For 4-substituted pyridinyl radicals, see: (a) Kosower, E. M. *Top. Curr. Chem.* **1983**, *112*, 117. (b) Ikegami, Y.; Muramatsu, T.; Hanaya, K.; Onodera, S.; Nakayama, N.; Kosower, E. M. *J. Am. Chem. Soc.* **1987**, *109*, 2876. (c) Kubota, S.; Ikegami, Y. *J. Phys. Chem.* **1978**, *82*, 2739 (d) Tripathi, G. N. R.; Su, Y.; Bentley, J.; Fessenden, R. W.; Jiang, P.-Y. *J. Am. Chem. Soc.* **1996**, *118*, 2245.

Chart 1

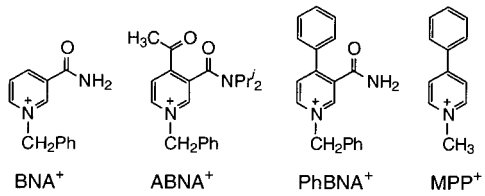

Among metal ions, rare-earth metal ions have attracted much attention as much more effective Lewis acids than divalent metal ions such as Mg^{2+} and Zn^{2+} in various carbon−carbon bond-forming reactions due to the strong affinity to carbonyl oxygen.[14] Scandium ion (Sc^{3+}) has recently been reported to be the strongest Lewis acid among metal ions.[15]

We report herein the complex formation between NAD^+ analogues [see Chart 1: 1-benzylnicotinamidiniumion (BNA^+) and 4-acetyl-*N*,*N*-diisopropyl-1-benzylnicotinamidinium ion ($ABNA^+$)] and scandium triflate ($Sc(OTf)_3$), which is shown to result in significant enhancement of electron-transfer reduction of the NAD^+ analogues for the first time. The $ABNA^+$ was newly prepared, since the one-electron reduced radical ($ABNA^•$) may be stable enough to be detected. The complex formation of $ABNA^•$ with Sc^{3+} has also been confirmed by successful detection of the ESR spectrum. The redox behavior of 1-benzyl-4-phenylnicotinamidinium ($PhBNA^+$) and the change due to the complexation with Sc^{3+} were also examined in comparison with that of 1-methyl-4-phenylpyridinium ion (MPP^+) which has no amide group like NAD^+ analogues (Chart 1). MPP^+ is known to cause Parkinsonian Syndrome,[16] and the redox reactivity of MPP^+ has merited considerable interest.[17] A comparison of the redox behavior between MPP^+ and the NAD^+ analogue thus also provides an interesting opportunity to clarify the role of amide group in the redox reactivity.

Experimental Section

Materials. Phenylmagnesium bromide was obtained from Kanto Chemical Co., Inc. Decamethylferrocene [$Fe(Cp^*)_2$] was obtained from Wako Pure Chemicals. Scandium trifluoromethanesulfonate, $Sc(OTf)_3$ (99%, FW = 492.16) was obtained from Pacific Metals Co. Ltd. (Taiheiyo Kinzoku). 1-Benzylnicotinamidinium perchlorate ($BNA^+ClO_4^-$) was prepared by following the literature procedure.[18] 1-Methyl-4-phenylpyridinium iodide (MPP^+I^-) was obtained from Sigma, which was converted to the perchlorate salt ($MPP^+ClO_4^-$) by addition of magnesium perchlorate in methanol and purified by recrystallization from methanol. Tris(2,2′-bipyridyl)ruthenium(II) chloride hexahydrate [$Ru(bpy)_3^{2+}$] was obtained from Aldrich. Acetonitrile (MeCN) and propionitrile (EtCN) were purified and dried by the standard procedure.[19] The sodium salt of the naphthalene radical anion (2.4×10^{-1} M in THF) was prepared by reduction of naphthalene (5.5 mmol) with sodium (5.0 mmol) under deaerated conditions in distilled THF at 298 K.[20]

Synthesis. $ABNA^+PF_6^-$ was synthesized as follows. First, 4-acetyl-*N*,*N*-diisopropylnicotinamide was prepared according to the literature.[21] $ABNA^+Cl^-$ was obtained by the reaction of 4-acetyl-*N*,*N*-diisopropylnicotinamide (0.40 g, 1.5×10^{-3} mol) with benzyl chloride (2 mL, 1.7×10^{-2} M) in methanol (5 mL) for 24 h. It was converted to the hexafluorophosphate salt ($ABNA^+PF_6^-$) by addition of potassium hexafluorophosphate to $ABNA^+Cl^-$ in water and purified by recrystallization from water (280 mg, 5.8×10^{-4} mol, 38%). ^{1}H NMR (300 MHz, CD_3CN) δ 8.88 (dd, J = 6.4, 1.3 Hz, 1H), 8.71 (d, J = 1.3 Hz, 1H), 8.28 (d, J = 6.4 Hz, 1H), 7.49 (m, 5H), 5.73 (s, 2H), 3.55 (m, 2H), 2.64 (s, 3H), 1.46 (d, J = 6.7 Hz, 6H), 1.08 (d, J = 6.7 Hz, 6H); ESI-MS m/z ($ABNA^+$) 339. Anal. Calcd for $C_{21}H_{27}N_2O_2PF_6$: C, 52.07; H, 5.62; N, 5.78. Found: C, 52.11; H, 5.63; N, 5.74. FT-IR (KBr) 1710, 1640 cm^{-1}. Mp 172.9−173.5 °C.

$PhBNA^+ClO_4^-$ was prepared by the following procedure. First, the phenylated BNAH (PhBNAH) was prepared by the Grignard reaction of PhMgBr with BNA^+Cl^-.[22] $PhBNA^+Cl^-$ was prepared by oxidation of PhBNAH by *p*-chloranil and addition of HCl according to the literature,[23] and it was converted to perchlorate salt ($PhBNA^+ClO_4^-$) by addition of sodium perchlorate to $PhBNA^+Cl^-$ in water,[24] and purified by recrystallization from water (380 mg, 1.2×10^{-3} mol, 39%). ^{1}H NMR (CD_3CN) δ 9.31 (dd, J = 6.4, 1.5 Hz, 1H), 8.85 (dd, J = 8.3, 1.5 Hz, 1H), 8.39 (dd, J = 8.3, 6.4 Hz, 1H), 7.04−7.68 (m, 10H), 5.86 (s, 2H);[25] ESI-MS m/z ($PhBNA^+$) 289. Anal. Calcd for $C_{19}H_{17}N_2O_5Cl\cdot H_2O$: C 56.10, H 4.71, N 6.89. Found: C 56.56, H 4.31, N 6.96. Mp 106.5−107.2 °C.

X-ray Structure Determination. $ABNA^+ClO_4^-$ was obtained from $ABNA^+Cl^-$ by conversion to the perchlorate salt by addition of sodium perchlorate in water. Single crystals of $ABNA^+ClO_4^-$ were obtained by evaporating methanol from a methanol solution of $ABNA^+ClO_4^-$ in the presence of an excess amount of water, although single crystals of $ABNA^+PF_6^-$ were not obtained. Data of X-ray diffraction was collected by Rigaku RAXIS-RAPID imaging plate two-dimensional area detector using graphite-monochromated Mo Kα radiation (λ = 0.71069 Å) to 2θ max of 55.0°. All the crystallographic calculations were performed by using teXsan software package of the Molecular Structure Corporation [teXsan: Crystal Structure Analysis Package, Molecular Structure Corp. (1985 and 1999)]. The crystal structure was solved by the direct methods and refined by the full-matrix least-squares. All non-hydrogen atoms and hydrogen atoms were refined anisotropically and isotropically. The experimental details include data collection, data reduction, and structure solution and refinement as well as the atomic coordinates and B_{iso}/B_{eq}, anisotropic displacement parameters.

Electrochemical Measurements. Electrochemical measurements of $ABNA^+PF_6^-$, $ABNA^+PF_6^-$−$Sc(OTf)_3$ complex, and $MPP^+ClO_4^-$ were performed on a BAS 100W electrochemical analyzer in deaerated MeCN containing 0.10 M $Bu_4N^+ClO_4^-$ (TBAP) as a supporting electrolyte at 298 K. The platinum working electrode was polished with BAS polishing alumina suspension and rinsed with acetone before use. The counter electrode was a platinum wire. The fast cyclic voltammetry

(14) (a) Imamoto, T. *Lanthanides in Organic Synthesis*; Katritzky, A. R., Meth-Cohn, O., Rees, C. W., Eds.; Academic Press: London, 1994. (b) Kobayashi, S. *Synlett* **1994**, 689. (c) Kobayashi, S. *Eur. J. Org. Chem.* **1999**, 15. (d) Molander, G. A.; Harris, C. R. *Chem. Rev.* **1996**, *96*, 307. (e) Shibasaki, M.; Sasai, H.; Arai, T. *Angew. Chem., Int. Ed. Engl.* **1997**, *36*, 1237.
(15) Fukuzumi, S.; Ohkubo, K. *Chem. Eur. J.* **2000**, *6*, 4532.
(16) (a) Markey, S. P.; Castagnoli, N.; Trevor, A. J.; Kopin, I. J. *MPTP: A Neurotoxin Producing a Parkinsonian Syndrome*; Academic Press: Orlando, FL, 1986. (b) Langston, J. W.; Ballard, P.; Tetrud, J. W.; Irwin, I. *Science* **1983**, *219*, 979. (c) Adams J. D.; Chang, M. L.; Klaidman, L. *Curr. Med. Chem.* **2001**, *8*, 809.
(17) (a) Brewster, M. E.; Kaminski, J. J.; Bodor, N. *J. Am. Chem. Soc.* **1988**, *110*, 6337. (b) Brewster, M. E.; Kaminski, J. J.; Huang, M. J.; Bodor, N. *J. Org. Chem.* **1990**, *55*, 2361. (c) Klaidman, L. K.; Adams, J. D.; Leung, A. C.; Kim, S. S.; Cadenas, E. *Free Radical Biol. Med.* **1993**, *15*, 169.
(18) Wallenfels, K.; Gellerich, M. *Chem. Ber.* **1959**, *92*, 1406.
(19) Perrin, D. D.; Armarego, W. L. F. *Purification of Laboratory Chemicals;* Butterworth-Heinemann: Oxford, 1988.
(20) (a) Closson, W. D.; Wriede, P.; Bank, S. *J. Am. Chem. Soc.* **1966**, *88*, 1581. (b) Corey, E. J.; Gross, A. W. In *Organic Syntheses: An Annual Publication of Satisfactory Methods for the Preparation of Organic Chemicals*; Bedejs, E., Ed.; John Wiley & Sons: New York, 1987; Vol. 65, p 166.
(21) Praly-Deprez, I.; Rivalle, C.; Huel, C.; Belehradek, J.; Paoletti, C.; Bisagni, E. *J. Chem. Soc., Perkin Trans. 1* **1991**, 3165.
(22) Anne, A. *Heterocycles* **1992**, *34*, 2331.
(23) (a) Anderson, A. G., Jr.; Berkelhammer, G. *J. Am. Chem. Soc.* **1958**, *80*, 992. (b) Mauzerall, D.; Westheimer, F. H. *J. Am. Chem. Soc.* **1955**, *77*, 2261.
(24) Fukuzumi, S.; Kondo, Y.; Mochizuki, S.; Tanaka, T. *J. Chem. Soc., Perkin. Trans. 2* **1989**, 1753.
(25) The lack of two protons of the amide ($-NH_2$) group in ^{1}H NMR data of $PhBNA^+ClO_4^-$ is attributed to the line broadening of the signal due to the exchange of proton in CD_3CN involving water.

measurements of $PhBNA^+ClO_4^-$ and $MPP^+ClO_4^-$ with $Sc(OTf)_3$ were performed on a BAS 100W electrochemical analyzer in deaerated MeCN containing 0.10 M TBAP as a supporting electrolyte at 298 K. The gold working microelectrode (i.d. = 10 mm, BAS) was polished with BAS polishing alumina suspension and rinsed with acetone before use. The counter electrode was a platinum wire. The second harmonic ac voltammetry (SHACV) measurements of $PhBNA^+ClO_4^-$, $PhBNA^+ClO_4^-$−$Sc(OTf)_3$ complex, $BNA^+ClO_4^-$, and $BNA^+ClO_4^-$−$Sc(OTf)_3$ complex were carried out with a BAS 100W electrochemical analyzer in deaerated MeCN containing TBAP as a supporting electrolyte at 298 K. The platinum working electrode was polished with BAS polishing alumina suspension and rinsed with acetone before use. The counter electrode was a platinum wire. The measured potentials were recorded with respect to an $Ag/AgNO_3$ (0.01 M) reference electrode. The E^0_{red} values (vs $Ag/AgNO_3$) are converted into those vs SCE by adding 0.29 V.

Spectral and Kinetic Measurements. The formation of the $Sc(OTf)_3$ complex with $ABNA^+PF_6^-$ and $BNA^+ClO_4^-$ was examined from the change in the UV−visible spectra of $ABNA^+PF_6^-$ and $BNA^+ClO_4^-$ in the presence of various concentrations of $Sc(OTf)_3$ by using a Hewlett-Packard 8453 diode array spectrophotometer. Kinetic measurements of electron transfer from $Fe(Cp^*)_2$ to $ABNA^+PF_6^-$ in the presence of $Sc(OTf)_3$ were performed on a UNISOKU RSP-601 stopped-flow rapid scan spectrophotometer with a MOS-type high-sensitive photodiode array at 298 K using a Unisoku thermostated cell holder designed for low-temperature experiments. Typically, rates of electron-transfer reactions from $Fe(Cp^*)_2$ (1.0×10^{-3} to 2.5×10^{-3} M) to $ABNA^+PF_6^-$ (1.0×10^{-4} M) in the presence of $Sc(OTf)_3$ ($5.0 \times 10^{-3} - 4.0 \times 10^{-2}$ M) were monitored by measuring the rise of the absorption band at λ = 792 nm due to $Fe(Cp^*)_2^+$. All kinetic measurements were carried out under pseudo-first-order conditions where the concentrations of $Fe(Cp^*)_2$ were maintained at greater than 10-fold excess of the concentrations of $ABNA^+PF_6^-$ at 298 K. Pseudo-first-order rate constants were determined by least-squares curve fits using a microcomputer.

Emission Quenching. Quenching experiments of the emission of $Ru(bpy)_3^{2+}$ were carried out on a SHIMADZU spectrofluorophotometer (RF-5000). The excitation wavelength of $Ru(bpy)_3^{2+}$ was $\lambda = 450$ nm in MeCN. The monitoring wavelength corresponded to the maximum of the emission band at $\lambda_{max} = 590$ nm. Typically, an MeCN solution was deaerated by argon purging for 8 min prior to the measurements. Relative emission intensities were measured for MeCN solutions containing $Ru(bpy)_3^{2+}$ (1.0×10^{-5} M), $BNA^+ClO_4^-$ (1.0×10^{-3} to 1.9×10^{-2} M) and $Sc(OTf)_3$ (0−1.0×10^{-1} M). There was no change in the shape, but there was a change in the intensity of the emission spectrum by the addition of a quencher (Q). The Stern−Volmer relationship (eq 1)

$$I_0/I = 1 + K_{SV}[BNA^+] \quad (1)$$

was obtained bewteen the ratio of the emission intensities in the absence and presence of $Sc(OTf)_3$ and the concentrations of $BNA^+ClO_4^-$ [BNA^+]. The emission lifetime[26] of $Ru(bpy)_3^{2+}$ was determined as τ = 850 ns in deaerated MeCN solution at 298 K by single-photon counting using a Horiba NAES-1100 time-resolved spectrofluorophotometer. The observed quenching rate constants k_q ($K_{SV}\tau^{-1}$) were obtained from the Stern−Volmer constants K_{SV} and the emission lifetime τ.

ESR Measurements. The ESR spectra of MPP•, ABNA•, and the ABNA•−Sc^{3+} complex were measured using a JEOL JES-FA100 ESR spectrometer. MPP• and ABNA• were generated by the reduction of $MPP^+ClO_4^-$ (1.0×10^{-2} M) and $ABNA^+PF_6^-$ (1.0×10^{-2} M) with naphthalene radical anion (6.0×10^{-3} to 1.0×10^{-2} M) in deaerated propionitrile (EtCN), respectively. The ESR spectra of MPP• and ABNA• were measured at various temperatures (−90 to −30 °C) using an attached VT (variable temperature) apparatus. The Sc^{3+} complex of ABNA• was generated by addition of $Sc(OTf)_3$ (1.0×10^{-2} M) to an EtCN solution of ABNA• (1.0×10^{-2} M) at 298 K. The ESR spectra were recorded under nonsaturating microwave power conditions. The magnitude of modulation was chosen to optimize the resolution and signal-to-noise (S/N) ratio of the observed spectra. The g value and hyperfine coupling constants (hfc) were calibrated using Mn^{2+} marker.

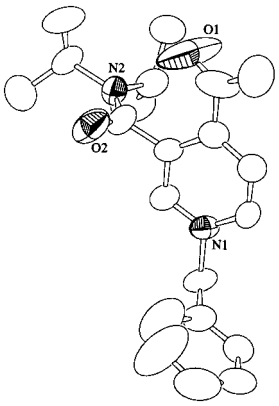

Figure 1. ORTEP drawing of $ABNA^+ClO_4^-$.

Scheme 1

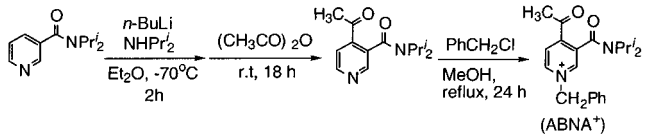

Theoretical Calculations. Density functional calculations were performed on a COMPAQ DS20E computer using the Amsterdam Density Functional (ADF) program version 1999.02 developed by Baerends et al.[27] The electronic configurations of the molecular systems were described by an uncontracted triple-ζ Slater-type orbital basis set (ADF basis set IV) with a single polarization function used for each atom. Core orbitals were frozen through 1s (C, O, N). The calculations were performed using the local exchange-correlation potential by Vosko et al.[28] and the nonlocal gradient corrections by Becke[29] and Perdew[30] during the geometry optimizations. Final geometries and energetics were optimized by using the algorithm of Versluis and Ziegler[31] provided in the ADF package and were considered converged when the changes in bond lengths between subsequent iterations fell below 0.01 Å.

Results and Discussion

Complexation between NAD⁺ Analogues and Sc^{3+}. The preparation of $ABNA^+ClO_4^-$ was carried out as shown in Scheme 1 (see Experimental Section). Single crystals of $ABNA^+ClO_4^-$ were obtained by evaporating methanol from a methanol solution of $ABNA^+$ in the presence of an excess amount of water. The crystallographic data are summarized in Supporting Information (Table S1), and the ORTEP drawing is shown in Figure 1.

The cyclic voltammograms of $ABNA^+$ in acetonitrile (MeCN) containing 0.10 M TBAP exhibited the reversible one-electron redox couples at −0.66 V (E^0_{red} vs SCE) as shown in Figure 2a. Addition of $Sc(OTf)_3$ (1.0×10^{-2} M) to an MeCN solution of $ABNA^+$ results in a remarkable positive shift in the E^0_{red}

(26) Bock, C. R.; Connor, J. A.; Gutierrez, A. R.; Meyer, T. J.; Whitten, D. G.; Sullivan, B. P.; Nagle, J. K. *J. Am. Chem. Soc.* **1979**, *101*, 4815.

(27) (a) Baerends, E. J.; Ellis, D. E.; Ros, P. *Chem. Phys.* **1973**, *2*, 41. (b) te Velde, B.; Baerends, E. J. *J. Comput. Phys.* **1992**, *99*, 84.
(28) Vosko, S. H.; Wilk, L.; Nusair, M. *Can. J. Phys.* **1980**, *58*, 1200.
(29) Becke, A. *Phys. Rev. A* **1988**, *38*, 3098.
(30) (a) Perdew, J. P. *Phys. Rev. B* **1986**, *33*, 8822. (b) Perdew, J. P. *Phys. Rev. B* **1986**, *34*, 7406.
(31) Versluis, L.; Ziegler, T. *J. Chem. Phys.* **1988**, *88*, 322.

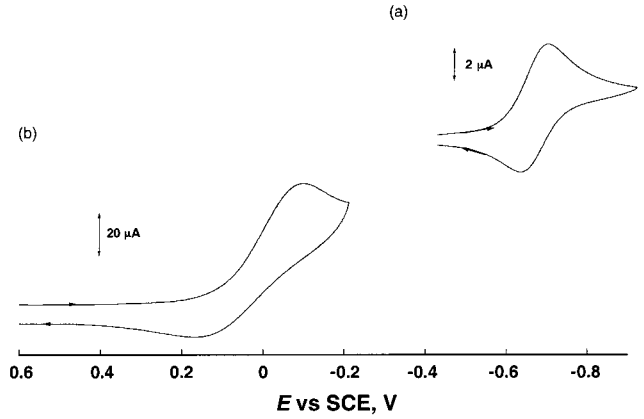

Figure 2. (a) Cyclic voltammogram of $ABNA^+PF_6^-$ (1.0×10^{-3} M) in the absence of $Sc(OTf)_3$ (sweep rate: 50 mV s^{-1}) and (b) cyclic voltammogram of $ABNA^+PF_6^-$ (1.0×10^{-3} M) in the presence of $Sc(OTf)_3$ (1.0×10^{-2} M) (sweep rate: 500 mV s^{-1}) in deaerated MeCN containing 0.10 M TBAP with a Pt working electrode at 298 K.

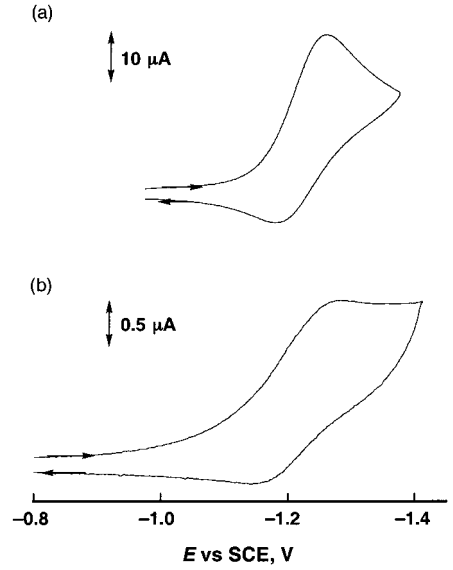

Figure 3. (a) Cyclic voltammogram of $MPP^+ClO_4^-$ (5.0×10^{-3} M) in the absence of $Sc(OTf)_3$ (sweep rate 200 mV s^{-1}) in deaerated MeCN containing 0.10 M TBAP with Pt working electrode at 298 K and (b) fast scan cyclic voltammogram of $MPP^+ClO_4^-$ (5.0×10^{-3} M) in the presence of $Sc(OTf)_3$ (1.0×10^{-2} M) (sweep rate 250 V s^{-1}) in deaerated MeCN containing 0.10 M TBAP with an Au working microelectrode at 298 K.

value (E^0_{red} vs SCE = 0.01 V) as shown in Figure 2b. Further addition of Sc^{3+} resulted in no further positive shift in the E^0_{red} value. In contrast to the case of $ABNA^+$, there is no change in the E^0_{red} value by the addition of Sc^{3+} (1.0×10^{-2} M) in the case of MPP^+ which has no amide or acetyl group (Figure 3). Thus, the remarkable positive shift in E^0_{red} may be caused by the complexation of $ABNA^+$ with Sc^{3+} through the amide group or the acetyl group or both.

To examine the effects of the amide and acetyl groups on the one-electron reduction potential of NAD^+ analogues, the E^0_{red} values of $PhBNA^+$ and BNA^+ were determined using a fast-scan cyclic voltammetry and a second-harmonic ac voltammetry, respectively (see Experimental Section). Although the redox wave of $PhBNA^+$ was irreversible at slow CV scan rates, it becomes reversible at fast scan rates (e.g., 167 V s^{-1}) using a microelectrode. The E^0_{red} values in the absence and presence of Sc^{3+} are listed in Table 1.[32] The E^0_{red} values of $PhBNA^+$ and BNA^+ are shifted to positive directions by 0.42 and 0.36 V in the presence of Sc^{3+} (1.0×10^{-2} M) as the case of $ABNA^+$, but the magnitude of the positive shift is smaller as compared to the case of $ABNA^+$ (0.67 V). This indicates that both amide and acetyl groups of $ABNA^+$ are involved in complexation with Sc^{3+}, resulting in the larger positive shift as compared to the case of $PhBNA^+$ or BNA^+, each of which has only one amide group.

Table 1. One-Electron Reduction Potentials (E^0_{red}) of $ABNA^+PF_6^-$, $MPP^+ClO_4^-$, $PhBNA^+ClO_4^-$, and $BNA^+ClO_4^-$ in the Absence and Presence of $Sc(OTf)_3$ Determined by the Cyclic Voltammetry and Second Harmonic ac Voltammetry

	E^0_{red} vs SCE	
	$[Sc^{3+}] = 0$ M	$[Sc^{3+}] = 1.0 \times 10^{-2}$ M
$ABNA^+$	−0.66[a]	0.01[b]
MPP^+	−1.21[c]	−1.21[d]
$PhBNA^+$	−1.12[e]	−0.70[f]
BNA^+	−1.08[g]	−0.72[f]

[a] Sweep rate: 50 mV s^{-1}. [b] Sweep rate: 500 mV s^{-1}. [c] Sweep rate: 200 mV s^{-1}. [d] Sweep rate: 250 V s^{-1}. [e] Sweep rate: 167 V s^{-1}. [f] Determined by SHACV. [g] Taken from ref 5a.

The complexation of $ABNA^+$ with Sc^{3+} is confirmed by the electronic spectral changes of $ABNA^+$ in the presence of Sc^{3+} in MeCN at 298 K (see Supporting Information, Figure S1). The new absorption band due to the $ABNA^+-Sc^{3+}$ complex appears at $\lambda_{max} = 282$ nm. The absorbance at $\lambda_{max} = 282$ nm increases with increasing Sc^{3+} concentration to approach a constant value (Figure 4a). This indicates that $ABNA^+$ forms a 1:1 complex with Sc^{3+}. The formation constant K for the Sc^{3+} complex of $ABNA^+$ is determined from a linear plot of $(A - A_0)^{-1}$ versus $[Sc^{3+}]^{-1}$ in Figure 4b, where A_0 and A are absorbances due to $ABNA^+$ and the Sc^{3+} complex, respectively. The linearlity of the plot in Figure 4b indicates the 1:1 complex formation of $ABNA^+$ with Sc^{3+}. From the slope and the intercept is obtained the K value as 530 ± 20 M^{-1}.[33] This value is consistent with the constant E^0_{red} value at $[Sc^{3+}] > 1.0 \times 10^{-2}$ M (vide supra), where most $ABNA^+$ molecules form the 1:1 complex with Sc^{3+}.

BNA^+ also forms a complex with Sc^{3+} as indicated by a red-shift of an absorption band of BNA^+ in the presence of Sc^{3+} ($\lambda_{max} = 319$ nm) (Figure S2). The formation constant K is also determined from the spectral change as 7.1 ± 1.0 M^{-1} (Figure S3) as listed in Table 2. The K value of $ABNA^+$ is much larger than the value of BNA^+. This is consistent with the larger positive shift in the E^0_{red} value of $ABNA^+$ due to complexation with Sc^{3+} as compared to that of BNA^+ (Table 1). The much larger K value of $ABNA^+$ results from the interaction of Sc^{3+} with both amide and acetyl groups of $ABNA^+$ in contrast to BNA^+ which has only one amide group.

Sc^{3+}-Promoted Electron Transfer. The significant positive shift in the one-electron reduction potential of NAD^+ analogues in the presence of Sc^{3+} suggests that an electron transfer from an electron donor to NAD^+ analogues which cannot occur thermodynamically becomes possible in the presence of Sc^{3+}. No electron transfer from decamethylferrocene ($Fe(Cp^*)_2$: E^0_{ox} vs SCE = −0.08 V)[34] to $ABNA^+$ occurs thermally in MeCN

(32) The change of E^0_{red} values depending on the diameter of the electrode, and the scan rate has been confirmed to be negligible in both CV and SHACV measurements of Sc^{3+}-free systems before measurements in the presence of Sc^{3+}.
(33) The overlapping absorption due to Sc^{3+} was subtracted to obtain absorbance due to the $ABNA^+-Sc^{3+}$ complex.
(34) Fukuzumi, S.; Mochizuki, S.; Tanaka, T. *Inorg. Chem.* **1989**, *28*, 2459.

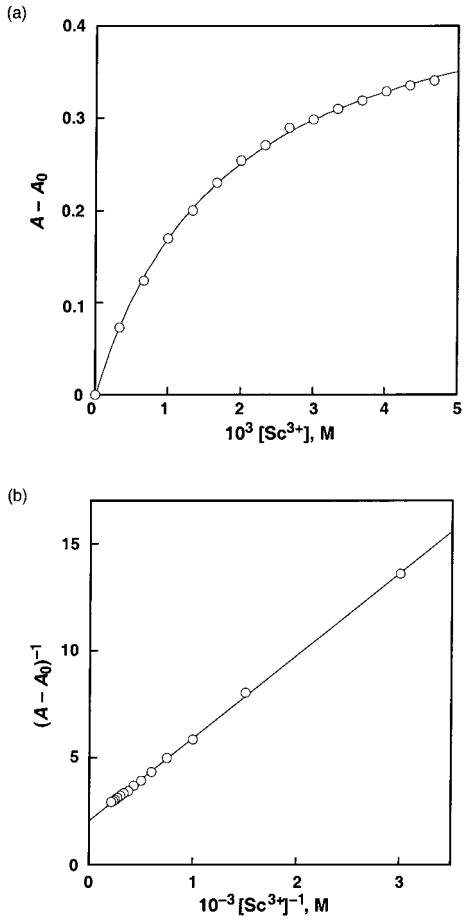

Figure 4. (a) Plot of $(A - A_0)$ vs $[Sc^{3+}]$ and (b) plot of $(A - A_0)^{-1}$ vs $[Sc^{3+}]^{-1}$ for the spectral change at $\lambda = 282$ nm due to the complexation of $ABNA^+PF_6^-$ with $Sc(OTf)_3$.

Table 2. Formation Constants of $ABNA^+PF_6^-$−$Sc(OTf)_3$ and $BNA^+ClO_4^-$−$Sc(OTf)_3$ (K), and Rate Constants (k_{et}) of Electron-Transfer Reaction from $Fe(Cp^*)_2$ to $ABNA^+PF_6^-$ and from $Ru(bpy)_3^{2+*}$ to $BNA^+ClO_4^-$ in the Presence of $Sc(OTf)_3$ in Deaerated MeCN at 298 K

	λ_{max}, nm	K, M^{-1}	K, M^{-1}	k_{et}, M^{-1} s^{-1}
$ABNA^+$−Sc^{3+}	282	5.3×10^2 [a]	5.5×10^2 [b]	1.4×10^3
BNA^+−Sc^{3+}	319	7.1[c]	6.0[d]	5.0×10^8

[a] Determined from the plot in Figure 4b. [b] Determined from the plots in Figure 5. [c] Determined from the plots in Figure S3. [d] Determined from the plots in Figure S6.

at 298 K as expected from the highly positive free-energy change of electron transfer ($\Delta G^0_{et} = 0.58$ eV). Addition of 1.0 mM of magnesium perchlorate ($Mg(ClO_4)_2$) or lutetium triflate ($Lu(OTf)_3$) to an MeCN solution of $ABNA^+$ (1.0×10^{-4} M) and $Fe(Cp^*)_2$ (1.0 mM) resulted in no change in the visible spectrum. In the presence of Sc^{3+} (1.0×10^{-2} M), however, electron transfer from $Fe(Cp^*)_2$ to $ABNA^+$ becomes exergonic ($\Delta G^0_{et} = -0.09$ eV), judging from the E^0_{red} value of $ABNA^+$ in the presence of Sc^{3+} (Table 1). In fact, addition of scandium triflate ($Sc(OTf)_3$: 1.0 mM) to an MeCN solution of $ABNA^+$ (1.0×10^{-4} M) and $Fe(Cp^*)_2$ (1.0 mM) resulted in formation of $Fe(Cp^*)_2^+$ as indicated by appearance of the absorption band due to $Fe(Cp^*)_2^+$ at $\lambda = 792$ nm.

The rate of formation of $Fe(Cp^*)_2^+$ obeys pseudo-first-order kinetics in the presence of a large excess of $Fe(Cp^*)_2$, and the pseudo-first-order rate constant increases linearly with $[Fe(Cp^*)_2]$

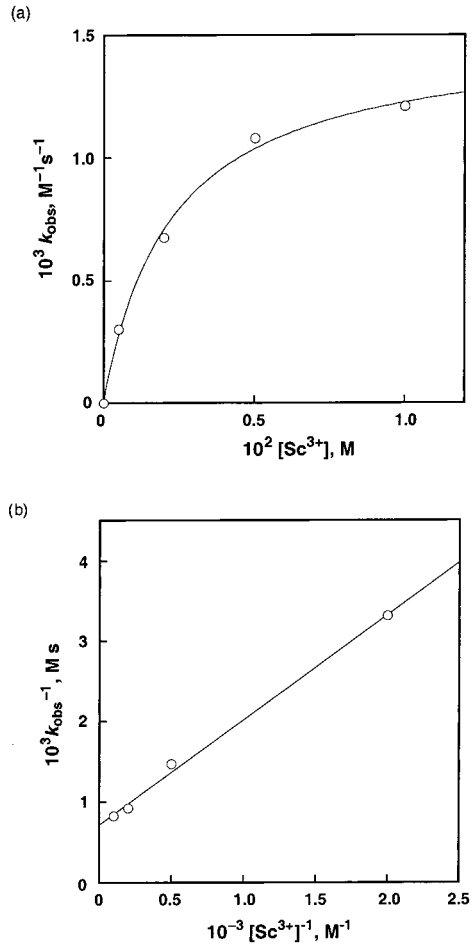

Figure 5. (a) Dependence of k_{obs} on $[Sc^{3+}]$ and (b) plot of k_{obs}^{-1} vs $[Sc^{3+}]^{-1}$ for electron transfer from $Fe(Cp^*)_2$ to $ABNA^+PF_6^-$ (1.0×10^{-4} M) in the presence of $Sc(OTf)_3$.

Scheme 2

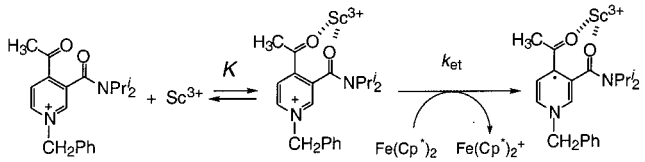

(Figure S4). The second-order rate constant of electron transfer (k_{obs}) determined from the linear plot increases with increasing Sc^{3+} concentration to approach a constant value (Figure 5a). Such a saturated dependence of k_{obs} on $[Sc^{3+}]$ indicates that the electron transfer occurs via the complex formed between $ABNA^+$ and Sc^{3+} as shown in Scheme 2.[35] According to this scheme the dependence of k_{obs} on $[Sc^{3+}]$ is given by eq 2,

$$k_{obs} = k_{et}K[Sc^{3+}]/(1 + K[Sc^{3+}]) \qquad (2)$$

where K is the formation constant for the complex between $ABNA^+$ and Sc^{3+}. From a linear relation between k_{obs}^{-1} and $[Sc^{3+}]^{-1}$ derived from eq 2 is determined the K value as 550 ± 90 M^{-1} and the k_{et} value as 1.4×10^3 M^{-1} s^{-1} (Table 2). The K value derived from the kinetic analysis of electron transfer agrees with the value determined directly from the spectral

(35) The shift of the stretching bands assignable to the amide group in IR spectra was observed due to the complexation of the amide group of $ABNA^+$ with Sc^{3+}; however, it was not possible to determine which atom (O or N) is responsible for coordination to Sc^{3+}.

Scheme 3

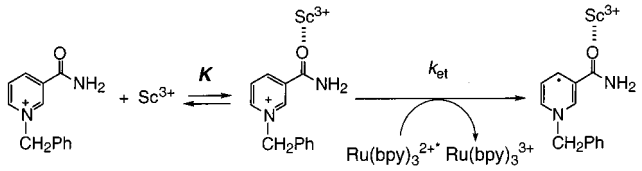

change of $ABNA^+$ in the presence of Sc^{3+} ($530 \pm 20\ M^{-1}$) in Figure 4. Such an agreement strongly supports the validity of Scheme 2.

The complex formation of BNA^+ with Sc^{3+} also facilitates the electron-transfer reduction of BNA^+ (vide infra). Although little emission quenching of $Ru(bpy)_3^{2+}$ (bpy = 2,2′-bipyridine) ($E^0_{ox} = -0.83$ V)[36] occurs by BNA^+ ($E^0_{red} = -1.08$ V)[5a] via photoinduced electron transfer,[5a] addition of Sc^{3+} to the $Ru(bpy)_3^{2+}$−BNA^+ system results in efficient emission quenching via electron transfer from the excited state of $Ru(bpy)_3^{2+}$ to BNA^+. The quenching rate constants (k_q) in the presence of various concentrations of Sc^{3+} were determined from the Stern−Volmer plot and the emission lifetime (850 ns) (Figure S5). The k_q value increases with an increase in $[Sc^{3+}]$ to approach a constant value (Figure S6a). Such a saturated dependence of k_q on $[Sc^{3+}]$ is also explained by the formation of 1:1 complex between BNA^+ and Sc^{3+} as the case of electron transfer from $Fe(Cp^*)_2$ to the $ABNA^+$−Sc^{3+} complex (Scheme 3). From a linear relation between $(k_q - k_{q0})^{-1}$ and $[Sc^{3+}]^{-1}$ (Figure S6b) derived from eq 2, where k_{obs} is replaced by $k_q - k_{q0}$, is determined the K value as $6.0 \pm 1.0\ M^{-1}$ and the k_{et} value as $5.0 \times 10^8\ M^{-1}\ s^{-1}$ (Table 2). The K value agrees with the value determined directly from the spectral change of BNA^+ in the presence of Sc^{3+} ($7.1 \pm 1.0\ M^{-1}$).

ESR Detection of MPP• and NAD• Radicals Analogue and Electron Self-Exchange. MPP• and ABNA• are relatively stable radicals, and they can be detected by ESR. To determine the self-exchange rate constant (k_{ex}) between MPP• and MPP^+ (Figure 6, Scheme 4), the ESR spectra of MPP• were measured in the presence of various concentrations of MPP^+ in EtCN. The hyperfine coupling constants of MPP• determined by computer simulation[7b,37,38] were similar to those of MPP• observed in 2-methyltetrahydrofuran.[39] The maximum slope line width (ΔH_{msl}) of each line increases linearly with an increase in the concentration of MPP^+ as shown in Figure 7. The rate constants (k_{ex}) of the electron-exchange reactions between MPP• and MPP^+ were determined using eq 3,

$$k_{ex} = (1.52 \times 10^7)\,(\Delta H_{msl} - \Delta H^0_{msl})/\{(1 - P_i)[MPP^+]\} \quad (3)$$

where ΔH_{msl} and ΔH^0_{msl} are the maximum slope line widths of the ESR spectra in the presence and absence of MPP^+, respectively, and P_i is a statistical factor.[40]

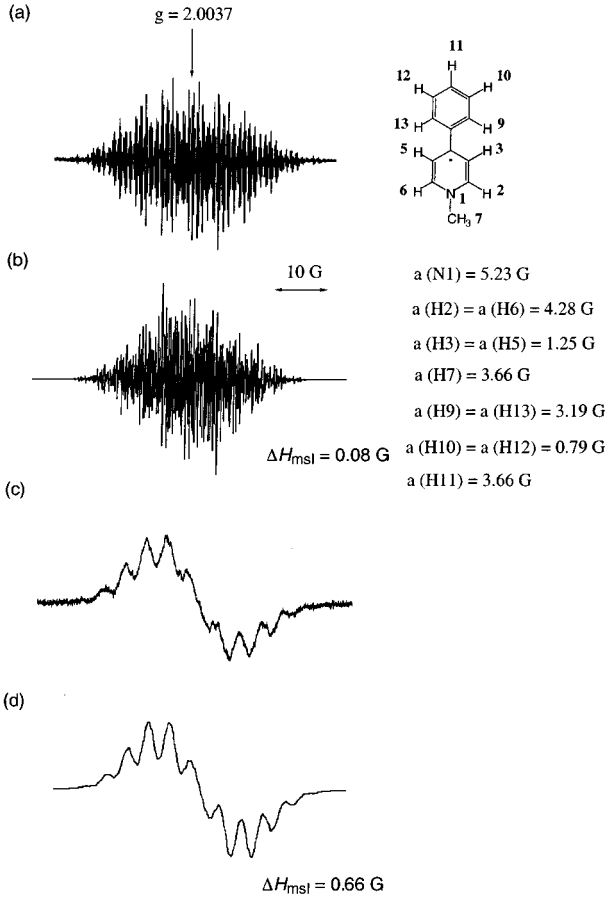

Figure 6. (a) ESR spectrum of MPP• generated by reduction of $MPP^+ClO_4^-$ with naphthalene radical anion in the absence of $MPP^+ClO_4^-$ in deaerated EtCN at 228 K and (b) the computer simulation spectrum with the listed hfc values. (c) ESR spectrum of the MPP• in the presence of $MPP^+ClO_4^-$ (4.2×10^{-3} M) in deaerated EtCN at 228 K and (d) the computer simulation spectrum with the listed hfc values.

Scheme 4

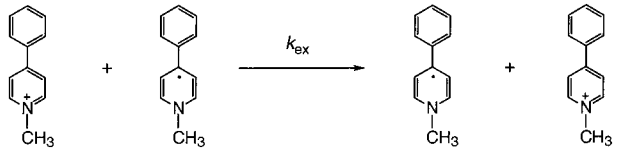

Figure 8a shows an ESR spectrum of ABNA• produced by the one-electron reduction of $ABNA^+$ with naphthalene radical anion in deaerated EtCN at 298 K. The hyperfine coupling constants (hfc) are determined by comparison of the observed spectrum with the computer-simulated spectrum as shown in Figure 8b. By comparing the hfc values with the spin densities obtained by the DFT (density functional theory) calculation,[7b,37,41] the largest spin density (0.242) is found at the C-4 position. This is consistent with the one-electron reduction products of NAD^+ as well as with the model compounds being identified as diasteroisomeric dimers with a symmetric 4,4′-linked structure.[42] The k_{ex} values for the electron exchange between ABNA• and $ABNA^+$ were also determined in a manner similar to those

(36) Kavarnos, G. J.; Turro, N. J. *Chem. Rev.* **1986**, *86*, 401.
(37) Gauld, J. W.; Eriksson, L. A.; Radom, L. *J. Phys. Chem. A* **1997**, *101*, 1352.
(38) The assignment of the hfc values is made by comparison with the hfc values predicted by the DFT calculation (triple-ζ Slater-type orbital set (frozen core: C (1s), N (1s), O (1s); ADF basis Set IV)). The calculated hfc values are obtained as 4.70 G (N1), 3.45 (H2, H6), 0.35 (H3, H5), 6.79 (H7), 2.08 (H9, H13), 0.30 (H10, H12), 2.64 (H11), which are used for assignment of the observed hfc values.
(39) Akiyama, K.; Kubota, S.; Ikegami, Y. *Chem. Lett.* **1981**, 469.
(40) (a) Chang, R. *J. Chem. Educ.* **1970**, *47*, 563. (b) Cheng, K. S.; Hirota, N. In *Investigation of Rates and Mechanisms of Reactions*; Hammes, G. G., Ed.; Wiley-Interscience: New York, 1974; Vol. VI, p 565.
(41) The assignment of the hfc values is made by comparison with the hfc values predicted by the DFT calculation (triple-ζ Slater-type orbital set (frozen core: C (1s), N (1s), O (1s); ADF basis Set IV)). The calculated hfc values are obtained as 1.76 (CH_3), 1.67 (H2), 1.11 (H5), 1.57 (H6), 3.04 (CH_2-Ph), 3.93 G (N1), which are used for assignment of the observed hfc values.
(42) Moracci, F. M.; Liberatore, F.; Carelli, V.; Arnone, A.; Carelli, I.; Cardinali, M. E. *J. Org. Chem.* **1978**, *43*, 3420.

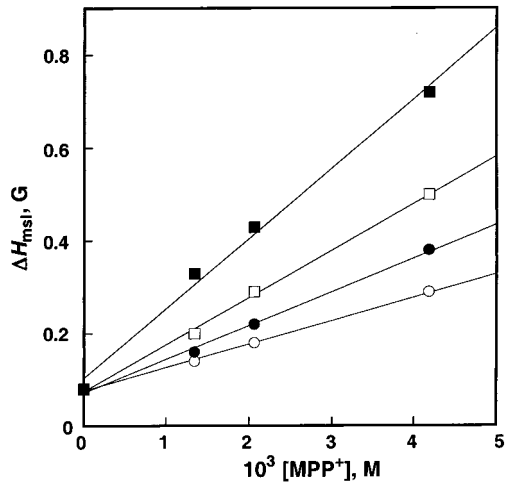

Figure 7. Plots of ΔH_{msl} vs [MPP⁺] for ESR spectra of MPP• in deaerated EtCN (○: 183 K, ●: 198 K, □: 213 K, ■: 228 K).

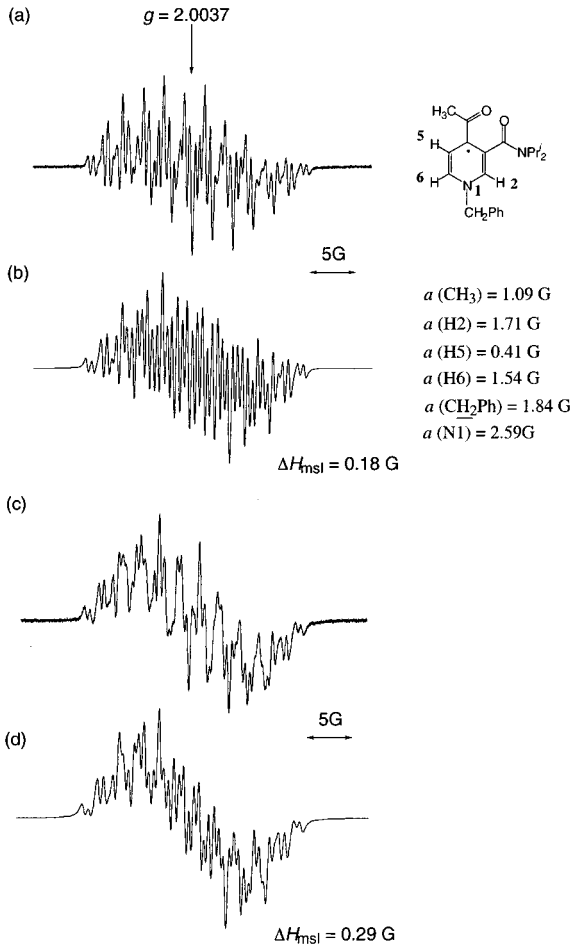

Figure 8. (a) ESR spectrum of ABNA• generated by reduction of $ABNA^+PF_6^-$ with naphthalene radical anion in the absence of $ABNA^+PF_6^-$ in deaerated EtCN at 298 K and (b) the computer simulation spectrum with the listed hfc values. (c) ESR spectrum of the ABNA• in the presence of $ABNA^+PF_6^-$ (2.0×10^{-3} M) in deaerated EtCN at 243 K and (d) the computer simulation spectrum with the listed hfc values.

for that between MPP• and MPP^+ (Figure 9), and the k_{ex} values of MPP• and ABNA• are listed in Table 3.

Arrhenius plots of log k_{ex} versus $1/T$ give the activation enthalpy ($\Delta H^{\ddagger}$) and activation entropy ($\Delta S^{\ddagger}$) (Figure S7). The $\Delta H^{\ddagger}$ values for MPP• and ABNA• were determined as 2.1 and 3.0 kcal mol^{-1}, respectively. The $\Delta S^{\ddagger}$ values for MPP• and ABNA• were determined as 5.1 and 6.2 cal K^{-1} mol^{-1}, respectively.

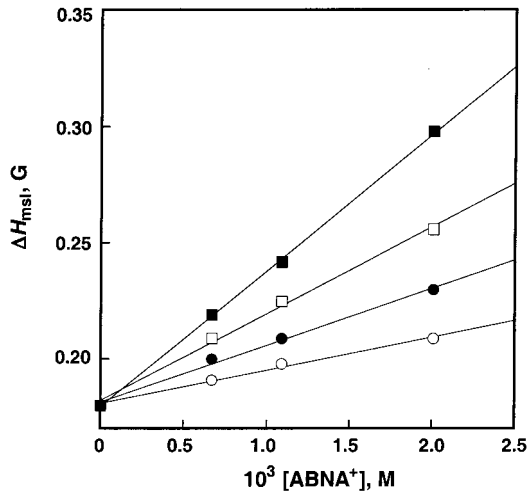

Figure 9. Plots of ΔH_{msl} vs [$ABNA^+$] for ESR spectra of ABNA• in deaerated EtCN (○: 198 K, ●: 213 K, □: 228 K, ■: 243 K).

Table 3. Rate Constants (k_{ex}) for Electron Self-Exchange between MPP• and $MPP^+ClO_4^-$, and between ABNA• and $ABNA^+PF_6^-$

T, K	MPP•/MPP⁺ k_{ex}, M^{-1} s^{-1}	ABNA•/ABNA⁺ k_{ex}, M^{-1} s^{-1}
183	8.0×10^8	–
198	1.2×10^9	2.2×10^8
213	1.7×10^9	3.8×10^8
228	2.6×10^9	5.9×10^8
243	–	9.3×10^8

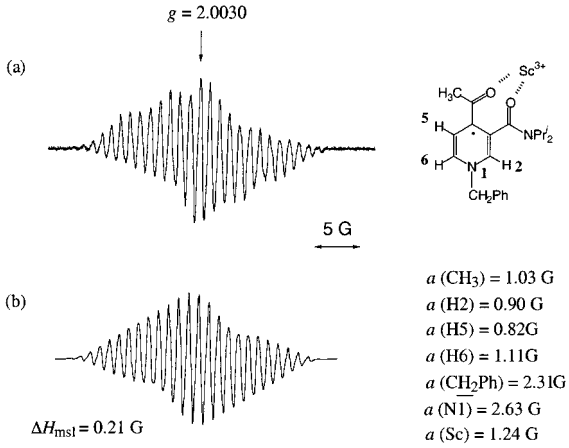

Figure 10. (a) ESR spectrum of the ABNA•-Sc^{3+} complex and (b) the computer simulation spectrum with the listed hfc values.

By addition of Sc^{3+} to the solution of ABNA•, the ESR spectrum of ABNA• is drastically changed to the spectrum in Figure 10a, which is well-reproduced by the computer simulation spectrum with the hfc values including a superhyperfine coupling due to one scandium nucleus (a(Sc) = 1.24 G) as shown in Figure 10b. The observation of such a superhyperfine coupling due to one scandium nucleus strongly indicates formation of the 1:1 complex between ABNA• and Sc^{3+}. The other hfc values are attenuated due to the complex formation of ABNA• with Sc^{3+}.

Conclusions

In conclusion, the rate of electron-transfer reduction of NAD^+ analogues is enhanced significantly by the complexation with

Sc^{3+} to produce stable $NAD^{\bullet}$ analogue−Sc^{3+} complex which has been successfully detected by ESR. This study thus provides valuable insight into the catalytic role of metal ions in controlling the redox reactivity of NAD^+ analogues.

Acknowledgment. This work was partially supported by a Grant-in-Aid for Scientific Research Priority Area (Nos. 11228205 and 13031059) from the Ministry of Education, Culture, Sports, Science, and Technology, Japan.

Supporting Information Available: An X-ray crystallographic file (CIF). X-ray crystallographic data (Table S1), UV−vis spectral change due to complex formation between $ABNA^+$ and Sc^{3+} (Figure S1), and between BNA^+ and Sc^{3+} (Figure S2), plots for determination of formation constant K (Figure S3), plots of pseudo-first-order rate constant vs $[Fe(Cp^*)_2]$ (Figure S4), Stern−Volmer plot (Figure S5), dependence of k_q on $[Sc^{3+}]$ (Figure S6), and Arrhenius plots (Figure S7) (PDF). This material is available free of charge via the Internet at http://pubs.acs.org.

JA0260364